Composite Structures 289 (2022) 115374

Contents lists available at ScienceDirect

Composite Structures

journal homepage: www.elsevier.com/locate/compstruct

The relation between in-plane fiber waviness severity and first ply failure in thermoplastic composite laminates

R.D.R. Sitohang [a,b], W.J.B. Grouve [b,*], L.L. Warnet [b], S. Wijskamp [a], R. Akkerman [a,b]

[a] ThermoPlastic composites Research Center (TPRC), Palatijn 15, 7521PN ENSCHEDE, NL, Netherlands
[b] University of Twente, Drienerlolaan 5, 7522NB ENSCHEDE, NL, Netherlands

ARTICLE INFO

Keywords:
Thermoplastic composites
Waviness
Bending
Defects
Mechanical testing
Compressive failure

ABSTRACT

The influence of in-plane fiber waviness on the first ply failure of quasi-isotropic thermoplastic composite laminates was investigated. The failure mode and stress at first failure were studied by using a four-point bending test and an end-loaded bending (ELB) test. The experimental results confirm that no undesirable stress concentration due to load introduction occurred in the ELB test, thereby supporting the use of this test as an alternative method to measure stress at failure. The experiments demonstrated that waviness severity affects stress at first failure and compressive damage development. The stress at first failure initially decreases with increasing maximum waviness angle and levels off as the angle starts exceeding 20°. These results reinforce the hypothesis from previous research which suggests that wavy ply compressive strength is less sensitive to changes in severity at larger angles. Furthermore, it was found that kinking failure was the dominant failure mode for maximum waviness angle up to about 45°. No kink band was observed in wavy regions with maximum angles above 45° when there was another wavy region with a lower maximum angle in the same specimen. This means that failure is not necessarily initiated at the location where waviness is most severe.

1. Introduction

1.1. Background

The demand for lighter aircraft structures to reduce carbon emissions is growing. One effective way to reduce the mass of aircraft is to use composite materials. Thermoplastic composites (TPCs) are ideal for this application, thanks to their high stiffness and strength-to-weight ratio, and particularly because of the possibility for process automation resulting from their melt-processable matrix. These advantages have been recognized by the aerospace industry and, as a result, the application of TPCs in commercial aircraft has been steadily growing over the past decades. Despite the gains made in manufacturing technologies, surface defects such as in-plane fiber waviness may still occur during parts manufacturing, i.e. during the consolidation or the forming process. These defects can cause uncertainty of the mechanical properties, particularly the compressive strength. This may then cause an unnecessarily high safety factor in the design of the aircraft structure, and consequently an increase of the structure's weight. Hence, efficient use of TPCs requires a proper understanding of the failure mechanisms and the mechanical properties of the composites with waviness defects.

Compressive strength is often a limiting design factor of composite materials for aircraft structures. The presence of waviness serves as a trigger to early compressive failure, as was observed in unidirectional (UD) [1–9] and multidirectional (MD) composites [10–14]. The kinking failure mechanism has been shown to be the dominant failure mode in UD composites and in some MD composites, depending on the severity of the defect and the stacking sequence [12–14]. This kinking mechanism is governed by the local shearing of the matrix due to the misalignment of fiber [15].

A previous study by the authors of this paper on quasi-isotropic (QI) laminates subjected to uniaxial compression showed that waviness in the ply oriented in loading direction caused early kink band formation in the wavy region, resulting in early failure of the laminate and significantly lower ultimate strength [14]. The studied waviness was found in one to three plies in 24-ply QI laminates with a maximum waviness angle (θ_{max}) between 23° to 60°, relevant to the defects from a stamp forming process. Similarly to earlier studies [10,11], the waviness caused a significant reduction of ultimate compressive strength. However, contrary to earlier work, the compressive strength of the specimens with waviness did not significantly depend on the maximum waviness angle for the range studied. Based on the maximum stress failure criterion, it can be shown that the compressive strength of a ply changes rapidly for small angles and then levels off as the angle further increases. This suggests that the first failure in the wavy ply

* Corresponding author.
E-mail address: w.j.b.grouve@utwente.nl (W.J.B. Grouve).

https://doi.org/10.1016/j.compstruct.2022.115374
Received 1 September 2021; Received in revised form 22 January 2022; Accepted 8 February 2022
Available online 26 February 2022

occurs at about the same stress level for the range of angles studied. To confirm whether this translates to the compressive strength of MD TPC laminates, further research focusing on the first ply failure of laminate with waviness is required.

Most published studies have used compression tests to evaluate the effect of waviness defects, which can lead to a sudden fracture [2,12,16]; this makes it difficult to monitor the initiation of damage and the failure mechanisms. Such sudden failure behavior was also found in the authors' previous study, which investigated waviness in laminates tested by using the combined loading compression (CLC) test method [14]. High-speed camera monitoring during the compression test used in that study confirmed that the first ply to fail was the wavy ply. However, for some of the specimens the damage initiation mechanism of the wavy ply is not yet clear, as it cannot be established solely from the fractography analysis of these specimens after testing. The initiated damage grows within a few milliseconds into full fracture, making it impossible to stop the test in time. In contrast with the compression test, the damage progression of composites under flexural loading is more gradual. It is thereby easier to monitor the damage evolution and to isolate the failure initiation by using a bending test.

1.2. Objective

This paper aims to investigate the influence of in-plane fiber waviness with a wide range of severities on the first ply failure of quasi-isotropic thermoplastic composite laminates. More specifically, it focuses on determining the ply compressive stress at which the first failure occurs when the laminate is subjected to bending, and identifying the mechanisms causing this failure.

1.3. Approach

Various test methodologies have been developed to measure the bending strength of composites. The generally accepted and standardized test methods are the three-point bending (3PB) and the four-point bending (4PB) test. The 4PB test is more suitable for the study of waviness defects due to the constant bending moment between the two loading cylinders. Although the 4PB test is commonly used to evaluate the bending strength of composites, it has the limitation of suffering from stress concentrations under the loading points which often causes premature failure of the specimen [17].

An alternative test method to overcome undesirable premature failure due to load introduction was developed by Fukuda et al. [17–19]. This test is in principle based on an eccentric compression loading condition. The term end-loaded bending (ELB) test is used in this paper to describe the compression bending test, to avoid confusion with the compression test. The previously developed method only measured the deflection at the mid-span of the specimen, and the authors did not report the failure location [17–20]. The bending moment with the ELB test method is not constant over the specimen length, with the maximum at the mid-span. Due to the presence of defects, the failure may not be located exactly in the mid-span. In such a case, the bending moment at the point of failure could not be determined solely from the mid-span deflection. To overcome this, a new measurement method by means of image analysis technique was implemented in this work to directly measure the curvature over the whole specimen length. The failure mode and the stress at first failure of several baseline (non-defective) samples obtained from the ELB and the 4PB tests were compared with the motivation to validate the use of the ELB test method.

One important aspect for an effect-of-defect study is to investigate the severity that is representative of the defects in actual parts. To this end, the specimen-manufacturing methods that directly mimic the mechanisms by which waviness is formed during TPC manufacturing processes were applied in this work. Two manufacturing procedures, i.e. press consolidation [21] and reverse forming method [22], were used to produce specimens whose waviness has a broad range of maximum waviness angles. The waviness investigated in this study is in the ply oriented in the loading direction. The stress at first failure of the specimens with waviness was subsequently assessed by using mainly the ELB test method. A limited number of specimens with waviness were also tested using the 4PB test method as a comparison. In both cases, the tests were stopped when the first failure was detected, to identify the damage mechanisms causing this failure. The failure mode was identified by fractography analysis using optical microscopy and scanning electron microscopy (SEM).

2. Experimental work

2.1. Material and specimens

Quasi-isotropic (QI) laminates were prepared from unidirectional carbon polyether-ether-ketone (PEEK) tapes known as Cetex® TC1200 from Toray Advanced Composites. A total of 24 plies were stacked in a $[0/45/90/-45]_{3s}$ layup to produce laminates with a nominal thickness of 3.4 mm. The UD tapes contain AS4 fibers with a fiber volume fraction of 59% [23]. As mentioned earlier, two manufacturing procedures were used to produce specimens with different levels of severity. The first was a press consolidation process which was performed using a well-chosen combination of tool material and release media, based on the findings from a study of the formation of fiber waviness during consolidation [21]. The second procedure was based on a stamp forming process, i.e. by a reverse forming method [22]. These two manufacturing procedures are described in more detail in the subsequent sections.

2.1.1. Press-consolidated specimens

UD tapes with the size of 300 mm × 300 mm were stacked in a picture frame mold between a combination of tool plates with release media. Two different materials were used as tool plates. The steel tool plates with the combination of Upilex 25S release films and Frekote 700-NC release agent were used to manufacture the baseline (non-defective) laminates, while the aluminum plates with Upilex 25S release films, but without any release agent, were used for the laminates with waviness (as listed in Table 1). The combination of a high coefficient of thermal expansion of the tool material and a high tool-ply coefficient of friction was found in an earlier study to promote the formation of fiber waviness during C/PEEK consolidation [21]. The UD tapes stack was then press-consolidated under 20 bar pressure with 20 min dwell time at 385 °C, and a cooling rate of 5 °C/min. Two laminates were produced for each of the settings.

Bending test coupons, 13 mm wide and 150 mm long, were cut from the manufactured laminates using a CNC milling machine. The test coupons were oriented parallel to the fiber direction of the surface ply. The specimen length was chosen such that a span-to-thickness ratio of 32:1 can be used for the 4PB test, according to the ASTM D7264 standard [24]. The specimen size was kept the same for both bending tests, 4PB and ELB tests.

2.1.2. Reverse-formed specimens

UD tapes were press-consolidated in the same way as the baseline laminate described in Section 2.1.1. The produced laminates were then cut using a water-cooled diamond-coated saw to obtain two 300 mm × 150 mm blanks for the subsequent stamp forming steps. These blanks were free of waviness prior to stamp forming.

Laminates with waviness were manufactured using a reverse forming method consisting of two stamp forming cycles (Fig. 1). Prior to the stamp forming process, the blanks were preheated in the IR oven at 465 °C for 300 s, to reach a midplane temperature of 390 °C. Three V-shaped matched metal toolings, as listed in Table 1, with different combinations of bend angles and inner radii were used in the first stamp forming step in order to vary the waviness severity

Fig. 1. Reverse forming steps to form in-plane waviness defects in a flat laminate. Reproduced from [14].

Table 1
Sample manufacturing methods. PC = press consolidation, RF = reverse forming. Release media: U = Upilex 25S, F = Frekote 700-NC, M = Marbocote 227CEE.

Sample	Processing method	Tool	Release	Tool geometry
Baseline-PC	Press consolidation	Steel	U + F	Flat
Waviness-PC	Press consolidation	Aluminum	U	Flat
Baseline-RF	Flat forming	Aluminum	M	Flat
Waviness-RF	Reverse forming	Steel	M	V-shape 90° bend
		Aluminum	M	V-shape 105° bend
		Aluminum	M	V-shape 120° bend

induced. All of the toolings were coated using the Marbocote 227CEE release agent. The V-shaped geometries used had a bend angle of 90°, 105°, and 120° with an inner radius of 6.4 mm, 8 mm and 10 mm, respectively. The V-shaped parts were formed by applying a nominal 40 bar consolidation pressure for 60 s while the part was cooled down to the tool temperature of 240 °C. The V-shaped parts were then reheated again in the IR oven for the subsequent flat forming step, with the same settings as before. The same forming parameters, except for pressure, were used for flattening the V-shaped parts to induce waviness. This second forming step was carried out by applying 100 bar consolidation pressure for 60 s. Two laminates were produced with the 90°-bend angle, one for each bending test method, and one laminate each for the other V-bend angles (the 105° and the 120°-bend). Finally, bending test coupons were cut from these laminates to the specimen dimension described earlier using a CNC milling machine.

Baseline laminates, as the non-defective reference, were manufactured using flat aluminum tools (Table 1) by following the same two stamp forming process cycles as previously described for the reverse forming procedure. These laminates therefore have the same pressure and thermal history as the ones with fiber waviness. Two laminates were produced, one for each bending test method. Finally, bending test coupons were cut from the baseline laminates to the specimen dimension described earlier.

2.2. Characterization of waviness parameters

Surface micrographs of each test coupon were taken with a Keyence VHX-5000 digital microscope with a resolution of 1.5 μm per pixel in order to quantify the waviness severity. Before image acquisition, the surface was prepared by applying a thin layer of sunflower oil on the surface to enhance the visibility of the fibers. Each test coupon typically had multiple wavy regions scattered across the surface. Separate micrographs were taken from each wavy region. The micrographs were processed with the high resolution misalignment analysis (HRMA) method developed by Wilhemsson et al. to trace the fibers [25]. A block size of 50 pixels × 50 pixels (75 μm × 75 μm) was used in this study. The maximum waviness angle (θ_{max}) and the wavelength (λ) were then measured for each wavy region. The largest θ_{max} from a given test coupon is defined as the overall θ_{max}. For example, the overall θ_{max} of the reverse-formed test coupon presented later in Fig. 5 is equal to 40°.

The wavelength was determined by performing a spectral analysis individually for each wavy region. The method proposed here utilizes Fourier transform to identify the spatial frequencies that can be found in the signal. This is done by transforming the result from the spatial domain, i.e. the fiber angle data along the horizontal direction, parallel to the 0° fiber orientation (Fig. 2(a)) to its frequency domain $X(k)$. The fiber angle, represented as $x(n)$ with a total of N number of blocks, is transformed to its frequency domain according to:

$$X(k) = \sum_{n=0}^{N-1} x(n) \exp\left(\frac{-2\pi j}{N} kn\right) \qquad \text{for } k = 0, 1, 2, \ldots, N-1 \tag{1}$$

The spatial frequency is kf_s/N, where the sampling frequency f_s equals the inverse of the spatial resolution, i.e. the block length of 75 μm. The wavelength is determined from the inverse of the dominant spatial frequency, i.e. the frequency at the largest magnitude, normalized to its maximum magnitude value. This can be visualized by determining the corresponding spatial frequency at the highest peak (Fig. 2(b)). The wavelength reported in this paper is the mean wavelength from each row of a given micrograph, which represents the dimension of the waviness in the fiber direction.

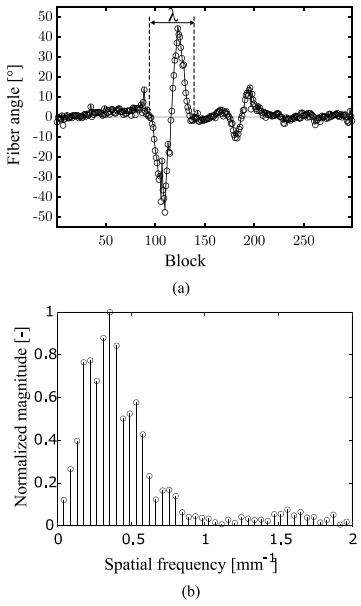

Fig. 2. Representation of the procedure to measure the wavelength. (a) Fiber angles displayed as a function of the number of blocks from a micrograph along the direction parallel to the nominal surface ply orientation. (b) The spatial frequencies from the fiber angles data in Figure a. The wavelength (λ) is calculated from the spatial frequency at the highest peak, where the wavelength equals 1/spatial frequency.

2.3. Mechanical testing procedure

2.3.1. Four-point bending test

The failure stress of the specimens was measured by means of four-point bending tests according to ASTM D 7264 [24]. The fiber direction

of the surface ply (0° ply) was along the length of the specimen, as the strength reduction due to fiber waviness is expected to be maximum for this loading direction. The wavy surface of the specimens was placed on the compression side. The support span length was set to 108 mm, resulting in a span-to-thickness ratio of 32:1. The loading cylinders were positioned equidistantly from the adjacent support, with the load span length equaling half of the support span length. The test was performed using an Instron 5982 universal testing machine equipped with a 10 kN load cell. It was carried out at a constant crosshead speed of 1 mm/min, which corresponds to the maximum strain rate of $2.1{\cdot}10^{-5}$ s^{-1} occurring at the outer surface and the mid-span length of the specimen. The test was stopped when the first failure was detected. The lamina compressive stress σ_{11} in the top outermost 0° ply for a pure bending state was calculated according to:

$$\sigma_{11} = Q_{11}\, z\, \kappa_x, \tag{2}$$

where z is the ply out-of-plane coordinate with respect to the laminate midplane, Q_{11} is the 11 element of the lamina stiffness matrix, and κ_x is the curvature along the x-axis (specimen length direction) [26]. The ply stress here is the stress in the material coordinates assuming the nominal fiber orientation of the corresponding ply. The UD tape material properties in Table 2 were used to determine the theoretical Q_{11} (125 GPa). The curvature κ_x can be obtained from the following relation:

$$\kappa_x = d_{11}\, M_x, \tag{3}$$

where M_x is the bending moment per unit width and d_{11} belongs to the laminate bending compliance matrix, calculated by $d_{11} = 12/(h^3 E_f)$, and where h is the specimen thickness and E_f is the measured flexural modulus [26]. The bending moment per unit width between the two loading noses is defined as $M_x = PL/8b$, calculated using the measured force P, the support span length L, and the specimen width b. The flexural secant modulus, i.e. the ratio of stress to corresponding strain at the strain of 0.003 [24], was determined from the test, according to:

$$E_f = \frac{0.17L^3 m}{bh^3}, \tag{4}$$

where m is the slope of the secant of the force–deflection curve. The deflection of the specimen was measured at the mid-span using a deflectometer.

Table 2
Material properties of AS4/PEEK UD tape for the ply stress calculation [14,23].

E_{11} [GPa]	E_{22} [GPa]	ν_{12} [–]	G_{12} [GPa]
124	10	0.33	4.2

2.3.2. End-loaded bending test

The second test method used to measure the failure stress was the end-loaded bending test using the setup shown in Fig. 3. The fiber direction of the outermost ply (0° ply) was oriented along the length of the specimen. The test coupon was clamped at both ends in fixtures that are fitted to ball bearings which then permit rotation of the test coupon ends. To facilitate predetermined direction of the deflection, the test coupon slots were positioned eccentrically such that there is an initial offset which is equal to half of the specimen thickness h (see Fig. 3) between the specimen's neutral axis and the axis of rotation of the bearing. In this way, similarly to the 4PB test method, the tension and compression sides can be predetermined. This ensures that the wavy surface is loaded primarily under compression during the test.

The test was carried out using an Instron 5982 universal testing machine equipped with a 10 kN load cell, at a constant crosshead speed of 1 mm/min until the first failure was detected. The maximum strain rate was $2.2{\cdot}10^{-5}$ s^{-1}, occurring at the outer surface and the mid-span

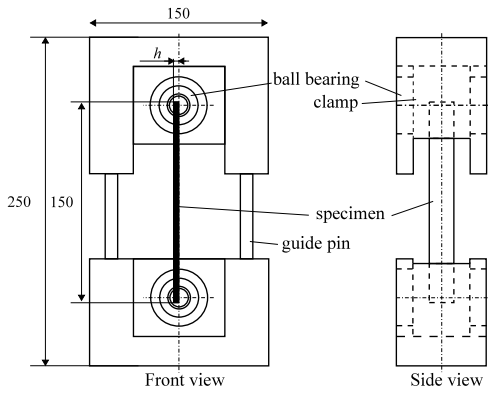

Fig. 3. Schematic of the end-loaded bending test setup. h is the specimen thickness. All dimensions are in mm.

length of the specimen. The specimen edge was monitored throughout the test by using a camera set viewing the specimen side (see Fig. 4). This camera was intended to evaluate the specimen curvature. It recorded videos at 2 frames per second (fps). Another camera was also used simultaneously monitoring the compression side at 240 fps during testing to observe the failure occurring. In addition, a limited number of tests was performed by using a high-speed camera (HSC) to monitor the damage sequence at a higher frame rate of 25,000 fps. The lighting for the HSC monitoring was too bright for the camera used to measure the curvature during the ELB test and disrupted the measurement.

Scoping experiments have indicated that the stress derived from deflection largely depends on the assumed initial position of the specimen's neutral axis, and the eccentricity, which also depends on the end rotation angle. Hence, the ply stress was calculated by using the directly measured curvature to avoid having to evaluate these end rotation angles. The curvature along the specimen length was automatically measured from the videos of the specimen side by image analysis. This works by tracing the edge of the specimen side, shown as the red line, at the region of interest (ROI) within the green rectangle in Fig. 4. The coordinates of the traced edge points in the z-direction (the horizontal coordinate in the image of the specimen side in Fig. 4) are expressed similarly to the general solution for eccentrically-loaded column buckling as:

$$z = A\sin(\sqrt{Pd_{11}/b}\, x) + B\cos(\sqrt{Pd_{11}/b}\, x) - C, \tag{5}$$

where x represents the coordinates along the specimen length, P is the measured force, d_{11} is the bending compliance of the laminate, and b is the specimen width. The three unknown coefficients A, B, and C are estimated by fitting the coordinates of the traced edge points to Eq. (5). The curvature along the specimen length κ_x (Fig. 4 top right) is then calculated according to:

$$\kappa_x = \frac{|z''|}{(1+(z')^2)^{3/2}}. \tag{6}$$

The measured curvature was validated by comparing it to the curvature determined by using strain gages. Two strain gages were bonded at the mid-span on both surfaces of a baseline (non-defective) specimen to determine the curvature. The difference between the optical and the strain gages measurements was within 1%.

The longitudinal stress (σ_{11}) of the outermost 0° ply in the principal material axes was calculated according to Eq. (2), assuming a negligible mid-plane strain from the axial compressive load. The influence of the compressive axial strain generated from the compressive force in the vertical direction, which was up to about 1000 N, was on average about 4% of the strain from the maximum curvature of each specimen. The ply stress was calculated assuming the nominal fiber orientation of the ply. The bending moment is not constant along the length of

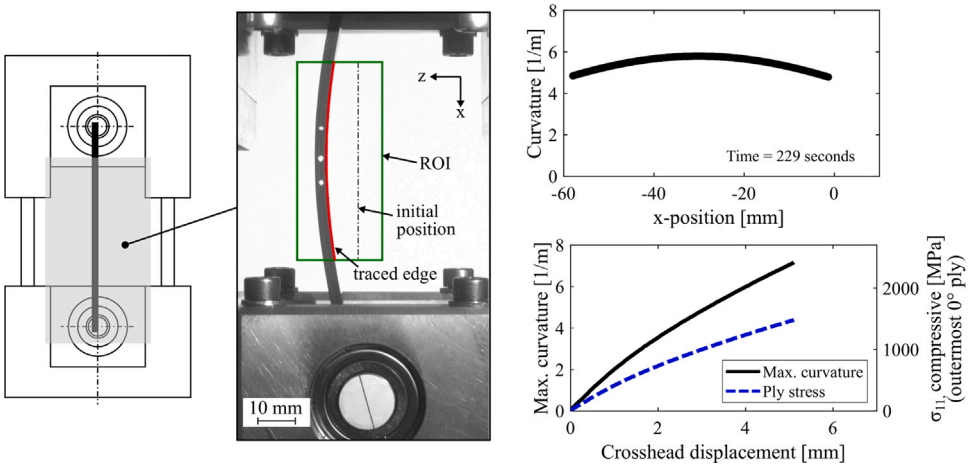

Fig. 4. Optical measurement of curvature from an image of the specimen side during ELB testing. The measured curvature along the specimen length is shown at the top right. The output from the image analysis is given on the bottom right, showing the maximum curvature and the outermost 0° ply longitudinal compressive stress (σ_{11}) from the whole test duration.

the specimen, leading to a non-constant curvature (as shown in Fig. 4). The position dependency of the curvature was taken into account when calculating the ply stress by considering the failure location.

2.3.3. Fractography

A number of specimens were selected for a closer post-failure analysis following the bending tests. The fractured surface was evaluated by means of optical microscopy using a Leica M125 microscope, and scanning electron microscopy with a JEOL JSM-7200F SEM.

3. Results and discussion

The characterization results of the waviness parameters are given first. The bending test results for the baseline samples and those with waviness are described next in separate sections, with both the 4PB and ELB test results given jointly for each type of sample. Lastly, the relation between waviness parameters and stress at first failure and the corresponding failure modes is discussed.

3.1. Waviness characterization results.

All press-consolidated (Waviness-PC) test coupons have wavy regions scattered throughout both the top and the bottom surfaces. Two to eight wavy regions (indicated by the ellipses in the micrograph in Fig. 5a) were observed to be scattered across the specimen length. Cross-sectional microscopy in Fig. 6a shows that the wavy fibers appear as ellipses with a small aspect ratio, i.e. major-axis-length over minor-axis-length in both outer 0° plies. The figure shows that the waviness extended through the entire thickness of the outer 0° plies, but did not propagate to the internal plies. For the bending test, the surface with the most pronounced waviness was placed on the compression side. Only the measured waviness parameters of this surface were reported here, as the failure is expected to occur on this side. Fig. 7 shows that the Waviness-PC sample represents the lower end of waviness severity, with the maximum waviness angle ranging between 3° to 13°. The wavy regions from the Waviness-PC sample have a mean wavelength of 3.3 mm.

The reverse-formed test coupons produced in this work have from one up to six wavy regions along their length (see Fig. 5b). These wavy regions were only observed on one surface. In this case, as illustrated in Fig. 6b, the waviness was only formed on the surface from the convex side of the V-shaped part [22]. Microscopy of the cross-section revealed no waviness in the internal plies. Fig. 8 shows the fiber angle distribution of the Waviness-RF specimens. Note the different scales between the vertical axes in Fig. 8 and in Fig. 7 for

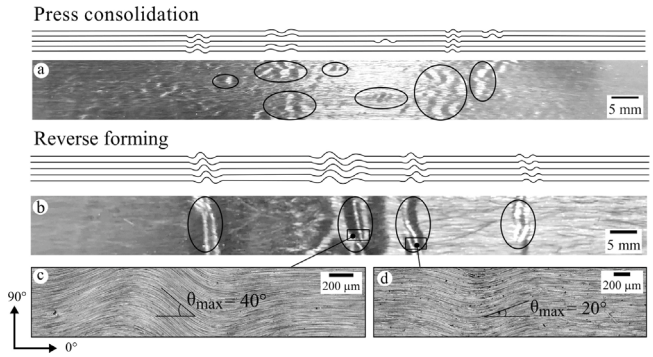

Fig. 5. Schematics of the in-plane waviness on the surface based on the typical surface micrographs of the test coupons manufactured by: (a) press consolidation and (b) reverse forming procedures. The surface micrographs (c) and (d) show examples of two wavy regions from the reverse-formed test coupon, with the maximum waviness angle (θ_{max}) shown at each wavy region.

the press-consolidated sample discussed earlier. Fig. 8 shows that the Waviness-RF sample has a much wider range of maximum waviness angle (θ_{max}) than the Waviness-PC sample, i.e. between 14° to 64°. The wavy regions from the Waviness-RF sample have a mean wavelength of 2.3 mm.

The baseline test coupons did not have any wavy regions, therefore no waviness parameters characterization was performed on these test coupons.

3.2. Bending test results of baseline samples

The typical force-versus-displacement curves obtained during 4PB and ELB testing are shown in Fig. 9a and b respectively. These tests were stopped when the first failure was detected, to inspect the specimen and identify the failure mechanisms. The ELB specimens showed a force–displacement behavior similar to that of an eccentrically-loaded column buckling response, where the force initially increases quickly with increasing displacement until a certain critical load and then levels off to a near-plateau (see Fig. 9b). The tested baseline samples have on average a flexural modulus of approximately 58.5 GPa. The difference between the moduli of the baseline samples manufactured by press consolidation and reverse forming processes was not significant. Moreover, the measured flexural modulus was fairly similar to the theoretical bending stiffness of 57.8 GPa, calculated using the classical

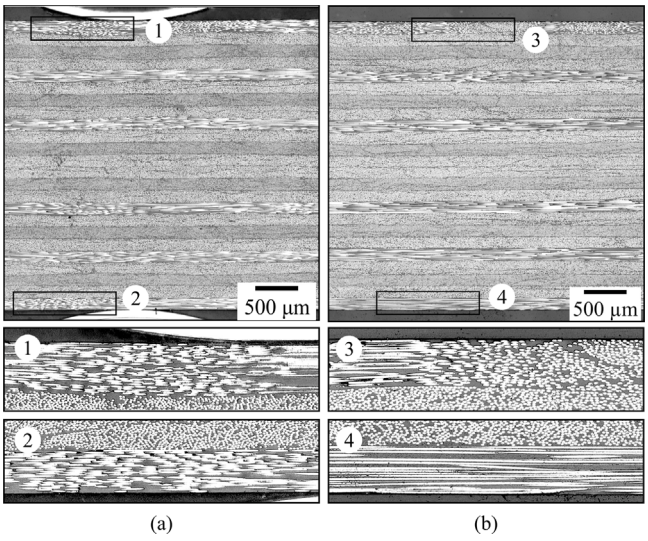

Fig. 6. Typical cross-sectional micrographs taken parallel to the fiber direction of the 0° ply from (a) the press consolidated and (b) the reverse-formed specimen with waviness. The numbers 1 and 3 indicate the micrographs from the top outermost 0° ply, and the numbers 2 and 4 indicate the bottom outermost 0° ply.

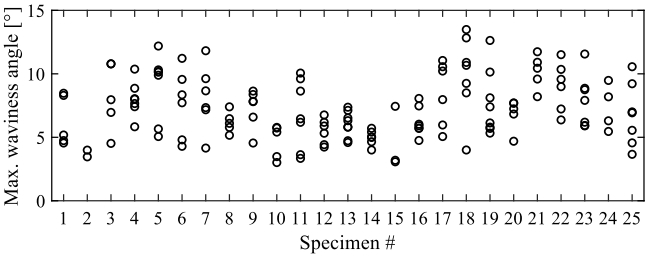

Fig. 7. Maximum waviness angles of the wavy regions in the Waviness-PC specimens. Each symbol represents a wavy region.

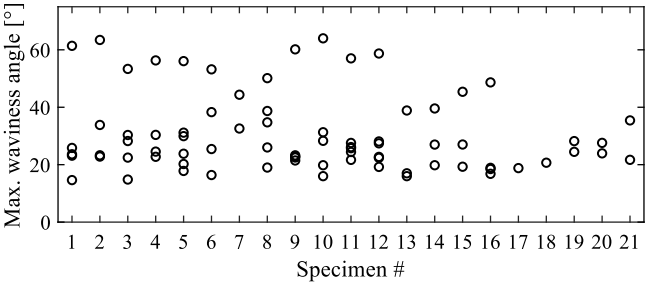

Fig. 8. Maximum waviness angles of the wavy regions in the Waviness-RF specimens. Each symbol represents a wavy region.

laminate theory (CLT), assuming the elastic constants given earlier in Table 2.

The 4PB specimens showed two types of failure depending on the failure location, i.e. at the loading nose or in the loading span. As can be seen in Table 3, the majority of these 4PB specimens showed compression failure at the loading nose; these are not considered as valid test results for failure stress measurement, as the stress state under the loading cylinder is unknown. The values shown in Table 3 for these specimens are thus not indicative of the strength of the material tested. For the Baseline-RF sample, in particular, all specimens failed at the loading nose, therefore no valid failure stress was determined from the 4PB test. In contrast to the specimens tested using the 4PB test, all baseline specimens tested using the ELB test showed failure

Table 3
Summary of failure type and ply compressive stress at first failure for the baseline samples. n = number of tested specimens.

Sample	Test method	Failure type[a]	n	Stress at first failure [MPa] (SD)
Baseline-PC	4PB	Type 1+2+3	3	1591 (69)
		Loading nose	4	1594 (160)
Baseline-PC	ELB	Type 1+2	2	2223 (283)
		Type 1+2+3	5	2089 (285)
Baseline-RF	4PB	Loading nose	6	1676 (118)
Baseline-RF	ELB	Type 1	2	1598 (123)
		Type 1+2+3	7	2267 (212)

[a]Loading span failure: type 1 = kinking, type 2 = ply splitting, type 3 = delamination.

in the loading span. These results confirm that no undesirable stress concentration due to load introduction occurred in the ELB test, thereby supporting the use of the ELB test as an alternative method to measure the stress at failure.

All tested baseline specimens that failed in the loading span, both the 4PB and the ELB specimens, showed failure on the compression side. As shown in Fig. 10, the failure can be distinguished into three types: kinking, which (in most cases) extends over the full width of the specimen (indicated with 1a), ply splitting (indicated with 2), and delamination (indicated with 3). The summary of the observed types of failure and the corresponding stress at first failure is presented in Table 3. The average ply compressive stresses at first failure for all the ELB baseline specimens, regardless of failure type, were 2127 MPa for the press-consolidated specimens and 2119 MPa for the reverse-formed specimens. The similar failure stress indicates that there is no significant influence of the different manufacturing processes on the ply failure stress. These values are significantly higher than the UD tape compressive strength obtained from the material datasheet (1300 MPa) [23]. The discrepancy can be explained by the difference in the type of tests used. The strength from the datasheet was measured by compression tests on UD composites, while the strength in this paper came from bending tests. As explained by Wisnom and Atkinson [27], a very high value of compressive strength can be reached in a bending test due to the presence of a through-the-thickness stress gradient.

Most specimens that failed in the loading span during 4PB and ELB testing showed a large load drop at the end of the test, but no complete through-thickness fracture (see Fig. 9). These specimens showed mixed types of failure (see Fig. 10), i.e. kinking (type 1), ply splitting (type 2) and delamination (type 3). The summary of the number of specimens for each corresponding failure type is given later in Table 4. The HSC footages in Fig. 11 show that the kinking failure preceded the ply splitting and the delamination. Therefore, ply splitting and delamination are considered as secondary mechanisms. A few baseline specimens showed a minor load drop, as shown in Fig. 9b. This behavior is associated with the specimens which failed only by kinking (type 1) or a combination of kinking and ply splitting (type 1+2). No delamination occurred in these cases.

3.3. Bending test results of samples with waviness

The typical force-versus-displacement curves obtained during 4PB and ELB testing of the specimens with waviness are presented in Fig. 12. Similarly to the tests of the baseline specimens, these tests were stopped when the first failure was detected. This is why in some cases only a very minor load drop can be seen at the end of the curves in Fig. 12. These results show a similar trend to that of the curves shown earlier for the baseline specimens. The tested samples with waviness have an average flexural modulus of approximately 57.6 GPa. The difference between the moduli of the wavy samples manufactured by press consolidation and reverse forming processes was (as expected) not significant. Compared to that of the baseline samples, it appears that

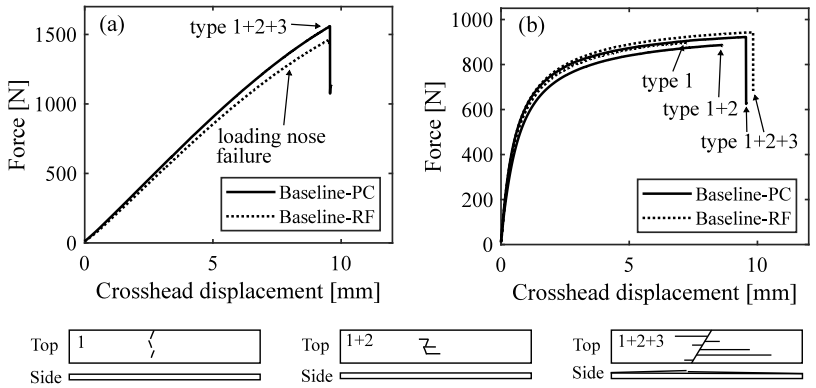

Fig. 9. Typical force–displacement curves from (a) 4PB and (b) ELB tests, performed until the first failure of the baseline specimens for each type of compression failure: kinking failure (type 1), ply splitting (type 2), and delamination (type 3).

Table 4
Summary of failure types. n = number of tested specimens.

Sample	Test method	n	Type 1[a]	Type 1+2[a]	Type 1+2+3[a]	Loading nose failure
Baseline-PC	4PB	7	0	0	3	4
Baseline-PC	ELB	7	0	2	5	0
Baseline-RF	4PB	6	0	0	0	6
Baseline-RF	ELB	9	2	0	7	0
Waviness-PC	4PB	14	2	2	5	5
Waviness-PC	ELB	11	2	4	5	0
Waviness-RF	4PB	5	5	0	0	0
Waviness-RF	ELB	16	16	0	0	0

[a]Type 1 = kinking, type 2 = ply splitting, type 3 = delamination.

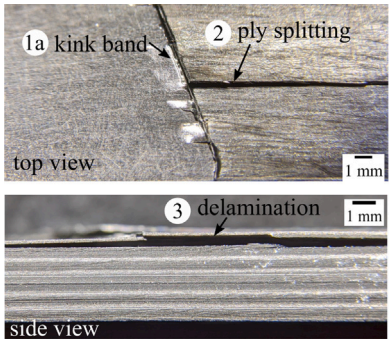

Fig. 10. Compressive failure modes of the baseline specimens.

the flexural modulus is not significantly influenced by the presence of waviness.

Table 4 shows that about one-third of the press-consolidated specimens with waviness from the 4PB tests failed under the loading nose. These specimens were excluded from the following discussion. By contrast, all the ELB specimens with waviness showed failure in the loading span, which again confirms the advantage of using the ELB test.

Similarly to the baseline specimens, the majority of the press-consolidated specimens with waviness showed mixed types of compression failure (as listed in Table 4), i.e. kinking, ply splitting (Fig. 13b), and delamination, with the failure localized at a single wavy region within a specimen. However, unlike the baseline specimens, in most cases, the kink bands did not extend over the full width of the specimen. A large load drop was observed at the end of the test of the specimen that failed by kinking and immediately followed by ply splitting and delamination (indicated as type 1+2+3 in Fig. 12). In this case, at the boundary of the kink band shown in Fig. 13b, the fiber fracture has propagated through the thickness of the wavy ply, indicating delamination. By contrast, only a minor load drop (Fig. 12b) was seen at the end of the test for the specimens that failed by either combined kinking and ply splitting (type 1+2), or only kinking (type 1). This indicates that delamination causes a significant loss of the load-bearing capability of the specimen.

Unlike the Waviness-PC specimens, all Waviness-RF specimens showed only kinking failure (see Fig. 13a), with fiber breakage visible at the boundary of the kink bands (see Fig. 14). These kink bands were observed in most cases at multiple wavy regions in a single specimen, although they did not grow into ply fracture and delamination. This also means that most Waviness-RF specimens showed failure in multiple locations. In contrast to the kinking failure observed in the baseline specimens, no kink bands (indicated as 1b in Fig. 13a) in the Waviness-RF specimens propagated across the entire width of the specimen. The sequence of the formation of kink bands between these wavy regions, however, was unknown since it was indistinguishable from the recorded images which have low magnification. Moreover, the failure was often barely audible and was accompanied by an indiscernible load drop. Testing by using a camera at higher magnification focusing on the wavy regions or having a specimen with less scattered wavy regions would help to better observe the failure mechanisms.

3.4. The relation between waviness parameters, stress at first failure, and failure mechanisms

The current section combines the characterization results from Section 3.1 and the results obtained from the bending experiments presented in Section 3.2 and Section 3.3 to discuss the effect of waviness.

As mentioned earlier, several kink bands were found at multiple wavy regions within a specimen for the Waviness-RF sample. However, the sequence of failure between the multiple wavy regions within a specimen cannot be identified from the recorded images. Only few specimens showed failure in a single wavy region. As such, only selected test results from the specimens for which the first wavy region to fail can be identified are given in Fig. 15. The graph shows the influence of the maximum waviness angle (θ_{max}) on the ply compressive stress at first

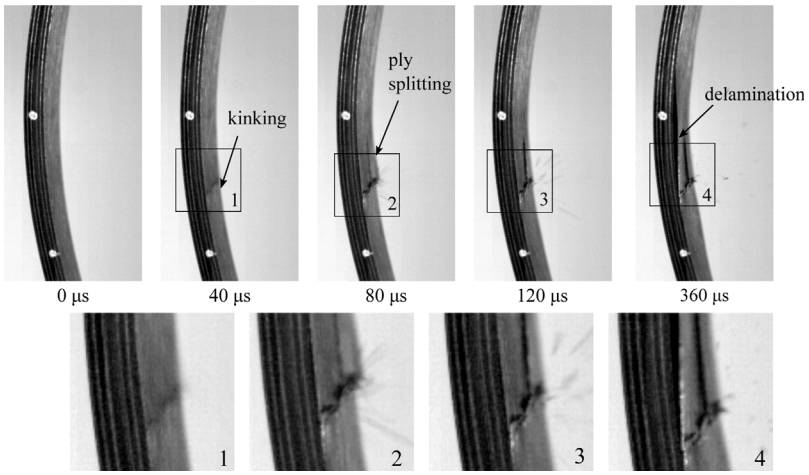

Fig. 11. High-speed camera images showing the damage sequence of a Baseline-RF specimen from the ELB test, with the close-up images at the bottom (numbers 1–4). The top white marker on the side of the specimen indicates the mid-span.

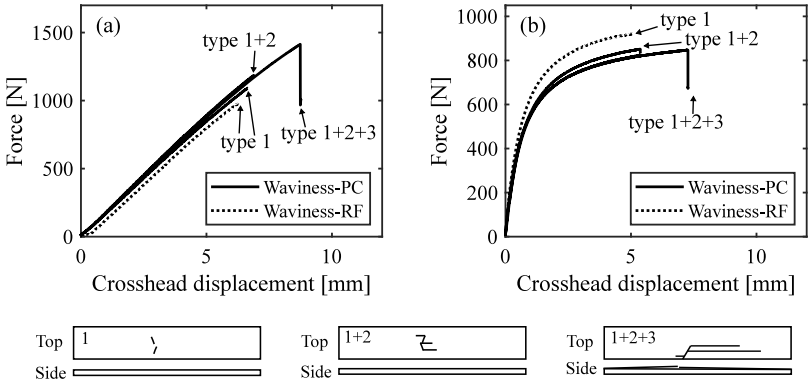

Fig. 12. Typical force–displacement curves from (a) 4PB and (b) ELB tests, performed until the first failure of the specimens with waviness for each type of compression failure: kinking failure (type 1), ply splitting (type 2) and delamination (type 3).

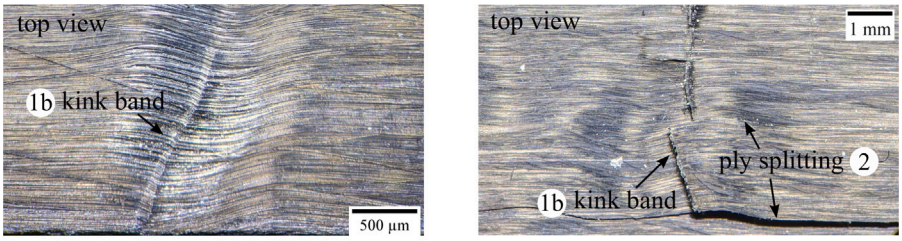

Fig. 13. Compressive failure modes of the specimens with waviness: (a) reverse-formed specimen, showing only kinking failure and (b) press-consolidated specimen, showing mixed types of failure: kinking and ply splitting.

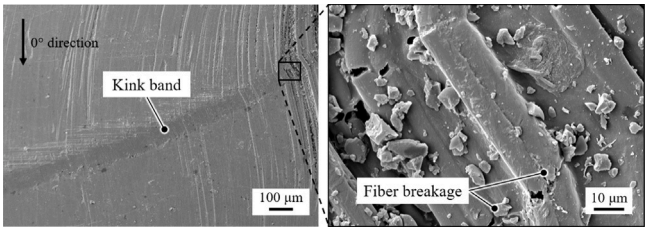

Fig. 14. SEM surface micrographs showing a kink band in the failed specimen that has waviness.

failure and the associated failure types. It seems that kinking failure initiation in the specimens with low maximum waviness angles tends to require a higher stress than that in the specimens with higher maximum angles. Furthermore, it is evident from Fig. 15 that waviness severity affects compressive damage development: the three mixed types of failure were observed for the lower θ_{max}, and only kinking failure was observed for the higher θ_{max}. This change in damage development seems to correspond with the difference in failure stress. The secondary failure mechanisms (ply splitting and delamination) occurring immediately after kinking were observed in the majority of the specimens that failed at a higher stress. These specimens failed at a larger compressive strain, as also reflected in the force–displacement curves presented earlier in Fig. 12. In this case, excess energy may have been released during the kinking failure. Then, this may trigger secondary damage

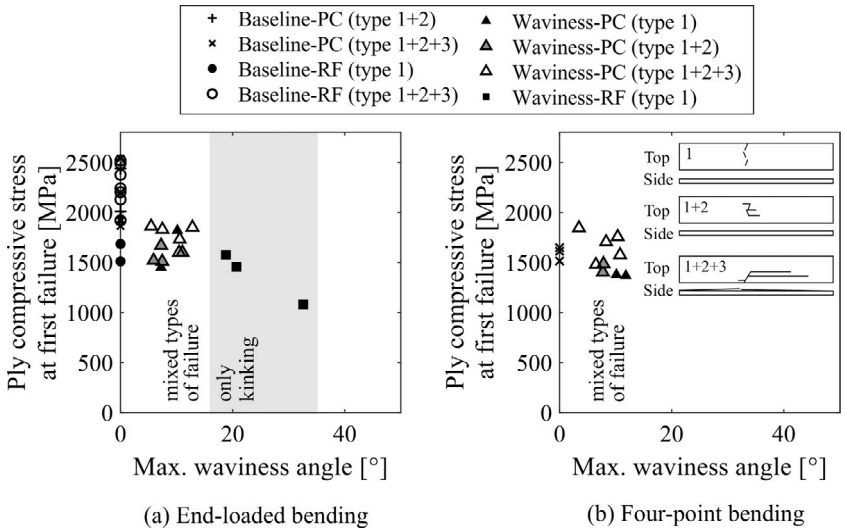

Fig. 15. Effect of waviness on ply compressive stress at first failure for the specimens which showed failure in a single location, as measured by: (a) ELB and (b) 4PB tests.

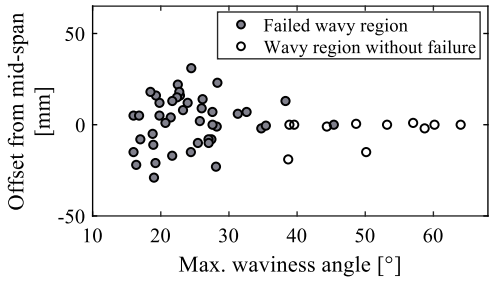

Fig. 16. Visual representation of the wavy region locations in the ELB test specimens from the Waviness-RF sample vs the maximum waviness angle (θ_{max}). For the sake of clarity, only the wavy regions with the largest θ_{max} and those closer to the mid-span (relative to the wavy region with the overall θ_{max} within the corresponding specimen) are shown here.

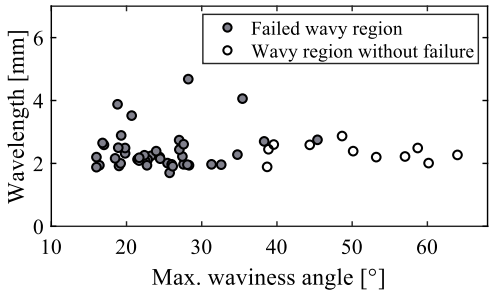

Fig. 17. Influence of wavelength and maximum waviness angle on compressive failure in Waviness-RF ELB specimens. Each symbol represents a single wavy region.

mechanisms which require more energy to be produced simultaneously with kinking.

For the ELB test method, the bending moment—hence the compressive stress—varies along the specimen length. For this reason, the location of each wavy region was also taken into account in the analysis, as represented in Fig. 16 as the offset distance from the mid-span. Note that the results shown in Fig. 16 were from all the Waviness-RF specimens, including those displaying multiple failure locations within a single specimen. It is evident from Fig. 16 that no kink band was observed at the wavy regions that have a maximum waviness angle larger than 45°, even when those wavy regions are located at the mid-span of the specimen. In such cases, the first failure was instead seen on the wavy region with a smaller θ_{max} that was further away from the mid-span than the wavy region with the largest θ_{max} in the same specimen. In addition, specimens with large overall θ_{max} values, i.e. between 53° to 63°, were also tested using the 4PB test to exclude dependency of the location of the wavy region. For the sake of brevity, the 4PB results are not presented in detail here as the same phenomenon was also observed, i.e. none of the Waviness-RF specimens showed failure at the wavy region with the largest θ_{max}. The 4PB results confirm that this observation was not influenced by the test method used, but rather the material behavior.

In conclusion, these results imply that the largest θ_{max} of a specimen above a certain threshold value does not necessarily cause the first failure when the laminate is subjected to bending. Instead, the first failure occurred in the other neighboring wavy regions that have smaller θ_{max} values. There are a few possible explanations for this phenomenon:

1. Failure is not governed by the maximum waviness angle in a region, but by some other waviness parameters.
2. Wavy regions with large fiber angles act as compliant regions, reducing local normal and shear stress.

Regarding the first point, Fig. 17 shows the influence of both wavelength and maximum waviness angle of each wavy region in Waviness-RF ELB specimens on the occurrence of compressive failure. Again, these results included those showing failure in multiple wavy regions within a single specimen. No obvious correlation between wavelength and the occurrence of failure can be established from the results shown here. The same conclusion was found from the analysis of the influence of the wavy region area. Hence for the sake of brevity, the characterization result of the other waviness parameter is not given here. In summary, these results do not support the first hypothesis.

Regarding the second point, in-plane waviness is known to give rise to an inhomogeneous stress distribution in the wavy region [14,28]. The inhomogeneity is due to the change in local fiber orientation, which causes a change in local stiffness. The region with a large fiber angle within the wavy region is locally more compliant than the surrounding material. This compliant region may cause a reduction of the stresses in the wavy region. A preliminary finite element (FE) analysis, using the modeling approach from the authors' previous work on compression testing [14], was performed to evaluate the stress state and the failure initiation in an idealized sinusoidal wavy region. This FE modeling approach has been previously validated by comparing the simulated and the measured strain fields from digital image correlation (DIC) experiments. The analysis shows that the dominant stress component which causes failure initiation in the wavy region is the in-plane shear stress in the principal material coordinate system. It was

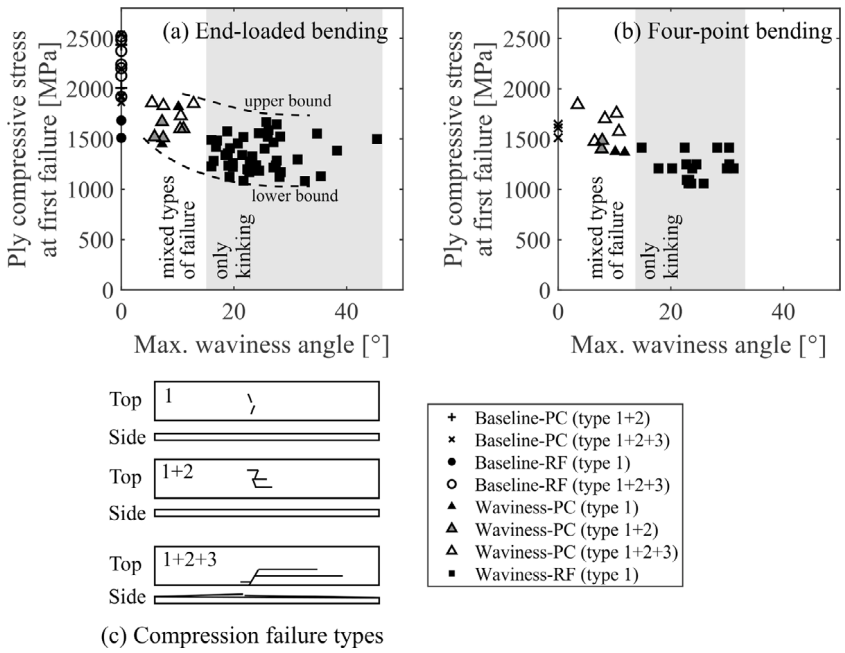

Fig. 18. Effect of waviness on ply compressive stress at first failure measured by: (a) ELB and (b) 4PB tests, and (c) the corresponding failure types. Note that there are multiple data points for the Waviness-RF specimens that were generated from the failure observed in multiple wavy regions from a single specimen.

found that for the same level of applied displacement, the in-plane shear stress in the wavy region with a large maximum angle (above 40°) can be less than that of the wavy region with a lower maximum angle. This implies that earlier failure can occur in the wavy region with a lower maximum angle, as opposed to the wavy region with the largest maximum angle within the same specimen. These findings from the FE results correspond with the experimental observations in the current study. Further research is required to gain more insight into the failure of the waviness with large severity. This can be performed, for example, by testing a specimen that has only one single wavy region with a large maximum angle.

As mentioned earlier, the sequence of failure between the multiple wavy regions within a single Waviness-RF specimen could not be identified. Nevertheless, the test results from these specimens may provide insight into the general trend of the influence of waviness parameters on the stress at first failure. The stresses at first failure for all the failed wavy regions within a single specimen are reported separately in Fig. 18 according to the local θ_{max} measured from the corresponding wavy region. Fig. 18 shows the influence of θ_{max} on ply compressive stress at first failure and the associated failure types from all tested specimens. The dashed lines in Fig. 18 indicate the lower and upper bounds of the ply compressive stress at failure at the region with large scatter. These data were generated under the assumptions that these failures occurred at the same force level and that the failure of a wavy region does not influence the stress state of the neighboring wavy region. The results presented in Fig. 18 show similar behavior regarding the influence of waviness severity on compressive failure types as that presented earlier from the specimens with a single failure location (Fig. 15).

The results from both the 4PB and ELB tests for the baseline specimens and those with waviness, including the specimens with multiple failed wavy regions, are combined in Fig. 19. The measured ply stress at first failure showed a large scatter, especially at the range of θ_{max} values between 7° to 32° , as indicated by the upper and lower bounds in Fig. 19. In general, as expected, the failure stress appears to decrease with increasing θ_{max}, with the largest reduction of failure stress up to about 50% with respect to the average baseline failure stress. The waviness with θ_{max} up to approximately 45° triggers an early failure initiation by kinking, thus lowering the failure stress. Despite the large

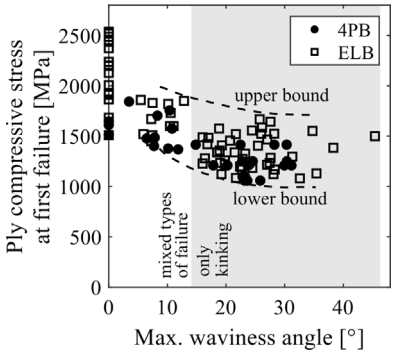

Fig. 19. Summary of the obtained experimental results from the four-point bending (4PB) and end-loaded bending (ELB) tests.

scatter seen in Fig. 19, it seems that the stress at first failure initially decreases with increasing maximum waviness angle, then levels off as the angle starts exceeding 20°. A similar conclusion was found from the previous work on uniaxial compression testing, where similar ultimate strengths were found for the specimens with θ_{max} between 23° to 60° [14]. These bending test results thus reinforce the hypothesis from our previous work: ply compressive strength is less sensitive to changes in severity at larger angles.

4. Conclusions

The influence of in-plane waviness defects in the ply oriented in loading direction on the first ply failure of quasi-isotropic C/PEEK laminates was investigated experimentally. The representative waviness defects were manufactured by a press consolidation process for low maximum waviness angles and a reverse forming method for the higher angles. The maximum waviness angles studied were between 3° to 64°. The wavy regions extended through the whole thickness of the surface 0° ply.

Ply compressive stress at failure was measured by using the end-loaded bending (ELB) and the four-point bending (4PB) test methods

such that the first ply failure can be isolated. The ELB test successfully yielded a consistent loading span failure for both the baseline (non-defective) and wavy specimens. Therefore, it can be concluded that the proposed ELB test method can provide a reliable strength measurement, without the presence of a premature failure due to loading point stress concentration as typically observed from 4PB tests.

The experimental results showed an influence of waviness severity on compressive damage development, i.e. kinking failure immediately followed by ply splitting and delamination for the smaller maximum waviness angles, and only kinking failure for the larger angles. Kinking failure was shown to be the dominant failure mode for maximum waviness angle up to about 45°, with fiber breakage observed at the boundary of the kink bands. No kink band was observed in the more severe wavy regions above 45° when there was another wavy region with a lower maximum angle in the same specimen. This means that the wavy region with the largest θ_{max} in a specimen does not necessarily cause the first failure. Although further research is required to investigate the failure of waviness with a large severity, a preliminary FEA in this work suggests that reduction of local stresses occurs at the wavy region with a large maximum waviness angle.

The specimens that showed kinking, ply splitting, and delamination failed at higher stresses than those that only exhibited kinking failure. Although the bending test results show a large scatter, the stress at first failure appeared to initially decrease with increasing maximum waviness angle but did not significantly change at the larger angles approximately above 20°. These results reinforce the hypothesis from previous research, which suggests that wavy ply compressive strength is less sensitive to changes in severity at the large angles.

CRediT authorship contribution statement

R.D.R. Sitohang: Conceptualization, Methodology, Investigation, Writing – original draft. **W.J.B. Grouve:** Conceptualization, Supervision, Writing – review & editing. **L.L. Warnet:** Conceptualization, Supervision, Writing – review & editing. **S. Wijskamp:** Supervision, Writing – review & editing. **R. Akkerman:** Project administration, Writing – review & editing.

Declaration of competing interest

The authors declare that they have no known competing financial interests or personal relationships that could have appeared to influence the work reported in this paper.

Data availability

The data that support the findings of this study are available from the corresponding author upon request.

Acknowledgments

The authors gratefully acknowledge the financial and technical support from the industrial and academic members of the ThermoPlastic composites Research Center (TPRC), as well as the support funding from the Province of Overijssel for improving the regional knowledge position within the Technology Base Twente initiative. The authors would like to thank Emiel van de Wetering for his contribution in developing the end-loaded bending test setup and Sylvio van Ditzhuijzen for his contribution in the press consolidation experiments.

References

[1] Highsmith AL, Davis JJ, Helms KL. The influence of fiber waviness on the compressive behavior of unidirectional continuous fiber composites. In: Composite materials: Testing and design (Tenth Volume). ASTM International; 1992.
[2] Joyce PJ, Moon TJ. In: Bucinell RB, editor. Compression strength reduction in composites with in-plane fiber waviness. West Conshohocken, PA: ASTM International; 1998, p. 76–96. http://dx.doi.org/10.1520/STP13267S.
[3] Wisnom MR, Atkinson JW. Fibre waviness generation and measurement and its effect on compressive strength. J Reinf Plast Compos 2000;19(2):96–110. http://dx.doi.org/10.1177/073168440001900201.
[4] Yokozeki T, Akakabe K, Aoki T, Kobiki A. Effects of process-induced fiber bundle waviness on the mechanical properties of carbon fiber reinforced thermoplastic composites. In: ECCM 2016 - Proceeding of the 17th European Conference on Composite Materials.
[5] Nair SN, Dasari A, Yue CY, Narasimalu S. Failure behavior of unidirectional composites under compression loading: effect of fiber waviness. Materials (Basel, Switzerland) 2017;10(8):909. http://dx.doi.org/10.3390/ma10080909.
[6] Wilhelmsson D, Gutkin R, Edgren F, Asp LE. An experimental study of fibre waviness and its effects on compressive properties of unidirectional NCF composites. Composites Part A: Appl Sci Manuf 2018;107:665–74. http://dx.doi.org/10.1016/j.compositesa.2018.02.013.
[7] Sun Q, Guo H, Zhou G, Meng Z, Chen Z, Kang H, Keten S, Su X. Experimental and computational analysis of failure mechanisms in unidirectional carbon fiber reinforced polymer laminates under longitudinal compression loading. Compos Struct 2018;203:335–48. http://dx.doi.org/10.1016/j.compstruct.2018.06.028.
[8] Mechin PY, Keryvin V, Grandidier JC, Glehen D. An experimental protocol to measure the parameters affecting the compressive strength of CFRP with a fibre micro-buckling failure criterion. Compos Struct 2019;211:154–62. http://dx.doi.org/10.1016/j.compstruct.2018.12.026.
[9] Yokozeki T, Takemura H, Aoki T. Numerical analysis on the flexural strength of unidirectional CFRTP composites with in-plane fiber bundle waviness. Adv Compos Mater 2020;29(1):89–100. http://dx.doi.org/10.1080/09243046.2019.1650322.
[10] Mandell J, Samborsky D, Wang L. Effects of fiber waviness on composites for wind turbine blades. In: 48th International SAMPE symposium, Vol. 48. 2003.
[11] Khan B, Potter KD, Wisnom MR. Simulation of process induced defects in resin transfer moulded woven carbon fibre laminates and their effect on mechanical behaviour. In: The 8th International Conference on Flow Processes in Composite Materials (FPCM8). 2006.
[12] Mukhopadhyay S, Jones MI, Hallett SR. Compressive failure of laminates containing an embedded wrinkle; experimental and numerical study. Composites Part A: Appl Sci Manuf 2015;73:132–42.
[13] Shipsha A, Hallström S, Burman M. Effect of stacking sequence and bundle waviness in quasi-isotropic NCF composites subjected to compression. Composites Part B: Eng 2019;178:107423. http://dx.doi.org/10.1016/j.compositesb.2019.107423.
[14] Sitohang RDR, Grouve WJB, Warnet LL, Akkerman R. Effect of in-plane fiber waviness defects on the compressive properties of quasi-isotropic thermoplastic composites. Compos Struct 2021;272:114166. http://dx.doi.org/10.1016/j.compstruct.2021.114166.
[15] Budiansky B, Fleck NA. Compressive failure of fibre composites. J Mech Phys Solids 1993;41(1):183–211.
[16] Wu C, Gu Y, Luo L, Xu P, Wang S, Li M, Zhang Z. Influences of in-plane and out-of-plane fiber waviness on mechanical properties of carbon fiber composite laminate. J Reinf Plast Compos 2018;37(13):877–91. http://dx.doi.org/10.1177/0731684418765981.
[17] Fukuda H. A new bending test method of advanced composites. Exp Mech 1989;29(3):330–5.
[18] Fukuda H, Katoh H, Uesugi H. A modified procedure to measure bending strength and modulus of advanced composites by means of compression bending. J Compos Mater 1995;29(2):195–207.
[19] Fukuda H, Itabashi M. Simplified compression bending test method for advanced composites. Composites Part A: Appl Sci Manuf 1999;30(3):249–56. http://dx.doi.org/10.1016/S1359-835X(98)00160-2.
[20] Fukuda H, Itabashi M, Wada A. Development of compression bending test method for advanced composites - A review, Vol. 11. 2004, http://dx.doi.org/10.1515/SECM.2004.11.2-3.169.
[21] Krämer ETM, Grouve WJB, Warnet LL, Koussios S, Akkerman R. Tool-ply interaction in the formation of waviness during c/peek consolidation. Composites Part A: Appl Sci Manuf 2021. http://dx.doi.org/10.1016/j.compositesa.2021.106327.
[22] Sitohang RDR, Grouve WJB, Warnet LL, Koussios S, Akkerman R. An experimental approach to reproduce in-plane fiber waviness in thermoplastic composites test coupons using a reverse forming method. J Compos Mater 2022;56(4):561–74. http://dx.doi.org/10.1177/00219983211026734.
[23] Toray Advanced Composites. Cetex TC1200 PEEK – Technical data sheet. 2019.
[24] ASTM. ASTM D7264 - Standard test method for flexural properties of polymer matrix composite materials, Vol. ASTM D7264. ASTM International; 2007.
[25] Wilhelmsson D, Asp L. A high resolution method for characterisation of fibre misalignment angles in composites. Compos Sci Technol 2018;165. http://dx.doi.org/10.1016/j.compscitech.2018.07.002.

[26] Gibson RF. Principles of composite material mechanics. CRC press; 2016.
[27] Wisnom MR, Atkinson JW. Constrained buckling tests show increasing compressive strain to failure with increasing strain gradient. Composites Part A: Appl Sci Manuf 1997;28(11):959–64. http://dx.doi.org/10.1016/S1359-835X(97)00067-5.
[28] Miyake T, Futamura M. Experimental investigation of fiber stress distribution in CFRP with in-plane fiber waviness. In: Turon A, Maimi P, Fagerström M, editors. 7th Eccomas Thematic Conference On The Mechanical Response Of Composites. p. 83–91.